

## Single *App* knock-in mouse models of Alzheimer's disease

Takashi Saito<sup>1,2</sup>, Yukio Matsuba<sup>1</sup>, Naomi Mihira<sup>1</sup>, Jiro Takano<sup>1</sup>, Per Nilsson<sup>1</sup>, Shigeyoshi Itoharu<sup>3</sup>, Nobuhisa Iwata<sup>1,4</sup> & Takaomi C Saido<sup>1</sup>

**Experimental studies of Alzheimer's disease have largely depended on transgenic mice overexpressing amyloid precursor protein (APP). These mice, however, suffer from artificial phenotypes because, in addition to amyloid  $\beta$  peptide (A $\beta$ ), they overproduce other APP fragments. We generated knock-in mice that harbor Swedish and Beyreuther/Iberian mutations with and without the Arctic mutation in the *APP* gene. The mice showed typical A $\beta$  pathology, neuroinflammation and memory impairment in an age-dependent manner.**

Identification of a protective mutation in the *APP* gene against sporadic Alzheimer's disease (AD)<sup>1</sup> has substantiated the A $\beta$  hypothesis that was originally based on the discovery of gene mutations that cause familial AD<sup>2</sup>. This hypothesis has led to the generation of a number of transgenic (Tg) mouse models that overexpress APP<sup>3,4</sup>, but these mice contain intrinsic problems that may induce artificial phenotypes (Supplementary Table 1 and Supplementary Fig. 1a). We overcame these problems by creating simple models that overproduce A $\beta$ <sub>42</sub> without overexpressing APP.

We manipulated the mouse *App* gene using a knock-in strategy (Supplementary Figs. 1b and 2) using Swedish (KM670/671NL)<sup>5</sup> and Beyreuther/Iberian (I716F) mutations<sup>6,7</sup>. The Swedish mutation elevates the total amount of A $\beta$ <sub>40</sub> and A $\beta$ <sub>42</sub>, whereas the Beyreuther/Iberian mutation increases the ratio of A $\beta$ <sub>42</sub> to A $\beta$ <sub>40</sub>. We first humanized the murine A $\beta$  sequence and inserted Swedish mutations (*App*<sup>NL</sup> mice). We then created another line that also possessed the Beyreuther/Iberian mutation (*App*<sup>NL-F</sup> mice), although putting the two independent mutations together may potentially exert unexpected effects. The presence of intron 16 was indispensable for correct expression of APP (data not shown).

Wild-type (*App*<sup>wt/wt</sup>), *App*<sup>NL/NL</sup> and *App*<sup>NL-F/NL-F</sup> mice generated equal amounts of APP and APP intracellular domain (AICD) (Supplementary Fig. 3a,b). Because Swedish mutations facilitate  $\beta$ -cleavage of APP<sup>8</sup>, the levels of C-terminal fragment  $\beta$  (CTF- $\beta$ ) increased similarly in *App*<sup>NL/NL</sup> and *App*<sup>NL-F/NL-F</sup> mice in a gene dose-dependent manner. These observations indicate that *App*<sup>NL/NL</sup> mice are relevant negative controls for *App*<sup>NL-F/NL-F</sup> mice. In contrast, APP-Tg mice (APP23) produced much higher levels of APP, CTF- $\beta/\alpha$  and AICD than *App*<sup>wt/wt</sup> and *App*<sup>NL-F/NL-F</sup> mice (Supplementary Fig. 4a).

The *App*<sup>NL-F/NL-F</sup> mice produced more A $\beta$ <sub>42</sub> than any of the other mice; the ratio of A $\beta$ <sub>42</sub>/A $\beta$ <sub>40</sub> was also highest in these mice (Supplementary Fig. 4b–e). The A $\beta$ <sub>42</sub> levels increased in an age-dependent manner (Fig. 1a), accompanying progressive A $\beta$  pathology (Fig. 1b). We detected initial deposition of A $\beta$  at 6 months in the *App*<sup>NL-F/NL-F</sup> mice (Supplementary Fig. 5) and at 12 months in APP-Tg mice (Supplementary Fig. 6a,b). Heterozygous *App*<sup>NL-F/wt</sup> mice exhibited cortical amyloidosis only after 24 months (Supplementary Fig. 7).

We next investigated the N- and C-terminal structures of A $\beta$  in the plaques of *App*<sup>NL-F/NL-F</sup> mice<sup>9</sup>. A $\beta$ <sub>1–42</sub> appeared as an initial species, followed by A $\beta$ <sub>3(pE)–42</sub> (Fig. 1c and Supplementary Fig. 5). A $\beta$ <sub>X–40</sub> was a minor species. This observation, consistent with human pathology (Supplementary Fig. 8a), implies that conversion of A $\beta$ <sub>1–42</sub> to A $\beta$ <sub>3(pE)–42</sub> occurs after deposition of A $\beta$ <sub>1–42</sub>. In contrast, the APP-Tg mice mainly accumulated A $\beta$ <sub>1–40</sub> (Supplementary Fig. 6c).

We observed accumulation of microglia and activated astrocytes (Fig. 1d), signs of neuroinflammation, around the A $\beta$  plaques. We also detected synaptic alterations, as indicated by losses of synaptophysin and PSD95 immunoreactivities (Fig. 1e) similar to those observed in AD brains (Supplementary Fig. 8b–d). We then examined memory function in the *App*<sup>NL-F/NL-F</sup> mice using the Y-maze test (Fig. 1f). The mutant mice showed impairment at 18 months, whereas *App*<sup>NL/NL</sup> mice were normal. This suggests that the increase in CTF- $\beta$  levels in the *App*<sup>NL-F/NL-F</sup> mice was not the cause of impairment, as *App*<sup>NL-F/NL-F</sup> and *App*<sup>NL/NL</sup> mice produce equal amounts of CTF- $\beta$  (Supplementary Fig. 3a,b). However, extremely high levels of CTF- $\beta$  may affect cognitive function in APP transgenic mice<sup>10</sup>.

Deficiency in calpastatin augments AD-associated pathology in APP-Tg mice<sup>11</sup>. The most notable feature of the double mutant is early lethality: half of them die by 10 weeks. We had thus argued that the calpain-calpastatin system might have a major role in AD pathogenesis. To validate these phenotypes, we generated *App*<sup>NL-F/NL-F</sup> and *App*<sup>NL/NL</sup> mice that were deficient in calpastatin (*App*<sup>NL-F/NL-F</sup> × *Cast*<sup>-/-</sup> and *App*<sup>NL/NL</sup> × *Cast*<sup>-/-</sup>). Calpastatin deficiency had no effect on the survival of *App*<sup>NL-F/NL-F</sup> and *App*<sup>NL/NL</sup> mice (Supplementary Fig. 9a). We also failed to reproduce other phenotypes such as increased tau phosphorylation and somatodendritic atrophy, as analyzed in a previously described manner<sup>11</sup> (data not shown). These are all likely artifacts caused by APP overexpression.

There were, however, a few confirmable phenotypes. Calpastatin deficiency exacerbated A $\beta$  amyloidosis in the *App*<sup>NL-F/NL-F</sup> mice (Supplementary Fig. 9b), as in APP-Tg mice. We also observed concomitantly higher microgliosis and astrocytosis in *App*<sup>NL-F/NL-F</sup> × *Cast*<sup>-/-</sup> mice than in *App*<sup>NL-F/NL-F</sup> mice (Supplementary Fig. 9c). Calpastatin deficiency increased the biochemical levels of A $\beta$  in *App*<sup>NL-F/NL-F</sup> mice, but not in *App*<sup>NL/NL</sup> mice (Supplementary Fig. 9d), suggesting that calpastatin deficiency affects processes associated with the deposition,

<sup>1</sup>Laboratory for Proteolytic Neuroscience, RIKEN Brain Science Institute, Wako-shi, Saitama, Japan. <sup>2</sup>Japan Science and Technology Agency, Saitama, Japan.

<sup>3</sup>Laboratory for Behavioral Genetics, RIKEN Brain Science Institute, Wako-shi, Saitama, Japan. <sup>4</sup>Department of Molecular Medicinal Sciences, Division of Biotechnology, Nagasaki University Graduate School of Biomedical Sciences, Nagasaki, Japan. Correspondence should be addressed to T.C.S. (saido@brain.riken.jp).

Received 5 January; accepted 12 March; published online 13 April 2014; doi:10.1038/nn.3697

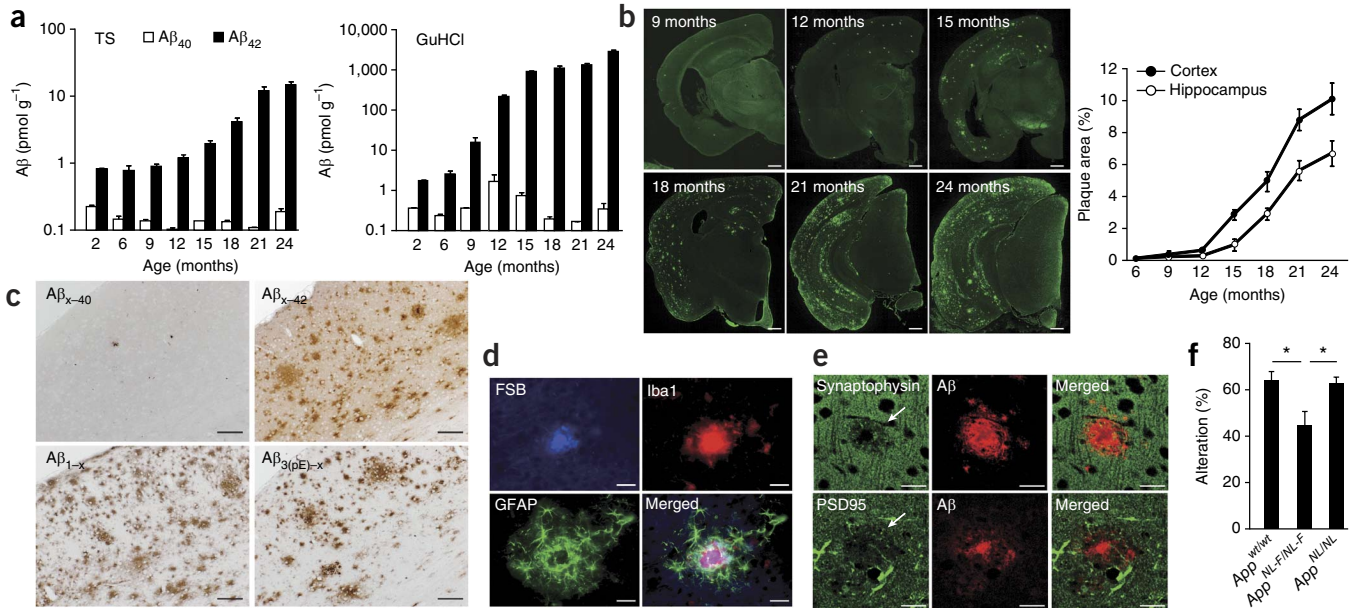


**Figure 1** Neuropathology and memory impairment of *App*<sup>NL-F/NL-F</sup> mice. **(a)** Biochemical quantities of A $\beta$ <sub>40</sub> and A $\beta$ <sub>42</sub> in *App*<sup>NL-F/NL-F</sup> brains. A $\beta$  levels in the Tris-HCl-buffered saline (TS) and GuHCl fractions of cortex from 2–24-month-old mice were quantified by sandwich ELISA. Data represent mean  $\pm$  s.e.m. ( $n = 4, 4, 5, 6, 6, 6, 4$  and  $6$  mice per indicated time point, respectively). **(b)** A $\beta$  pathology in *App*<sup>NL-F/NL-F</sup> brains. Brain sections from 9–24-month-old *App*<sup>NL-F/NL-F</sup> mice were immunostained with antibody to A $\beta$  (4G8). Plaque areas were quantified as indicated in the graph on the right ( $n = 4, 5, 6, 6, 6, 4$  and  $6$  mice per indicated time point, respectively). Scale bars represent  $500 \mu\text{m}$ . **(c)** N- and C-terminal structures of A $\beta$  in the *App*<sup>NL-F/NL-F</sup> brain. Brain sections from 24-month-old *App*<sup>NL-F/NL-F</sup> mice ( $n = 4$ ) were immunostained with endo-specific antibodies as indicated. Scale bars represent  $100 \mu\text{m}$ . **(d)** Neuroinflammation in *App*<sup>NL-F/NL-F</sup> mouse brains. Inflammatory responses were detected by triple staining using fluorostyryl benzene (FSB), antibody to GFAP and antibody to Iba1 as markers of cored A $\beta$  plaque, astrocytosis and microgliosis, respectively. Cortical immunoreactivities were quantified as shown in **Supplementary Figure 3c**. Scale bars represent  $25 \mu\text{m}$ . **(e)** Synaptic alterations in *App*<sup>NL-F/NL-F</sup> mouse brains. Double staining was performed using 4G8 antibody with a presynaptic marker (antibody to synaptophysin) and with a postsynaptic marker (antibody to PSD95). Scale bars represent  $10 \mu\text{m}$ . **(f)** Memory impairment in *App*<sup>NL-F/NL-F</sup> knock-in mice. The Y-maze test was performed using 18-month-old mice. Data represent mean  $\pm$  s.e.m. ( $n = 10$ , one-way ANOVA with Sheffe's *F* test,  $*P < 0.05$ ).

rather than the generation, of A $\beta$ . Furthermore, calpastatin deficiency increased the memory impairment of *App*<sup>NL-F/NL-F</sup> mice by 3 months (**Supplementary Fig. 9e**), consistent with accelerated A $\beta$  pathology.

Some of the phenotypes that we observed in APP-Tg mice therefore turned out to be artifacts, presumably resulting from high levels of APP and non-A $\beta$  fragments, whereas other phenotypes did not. This makes *App*<sup>NL-F/NL-F</sup> mice convenient tools for distinguishing facts from artifacts in the phenotypes thus far reported using APP-Tg mice crossbred with other genetically modified mice. In particular, the roles of tau<sup>12</sup> and apolipoprotein E<sup>13</sup> are important. It is also possible that some of the clinical trials of candidate AD therapeutics failed because the researchers immediately progressed from APP-Tg mice to humans without any additional validation.

We also generated another line of mice that carry the Arctic mutation<sup>14,15</sup> in addition to the Swedish and Beyreuther/Iberian mutations (*App*<sup>NL-G-F</sup>) (**Supplementary Fig. 1b**). *App*<sup>NL-G-F/NL-G-F</sup> mice exhibited APP expression and processing identical to that of *App*<sup>NL-F/NL-F</sup> mice (**Supplementary Fig. 10a,b**). However, this mutation, located in the middle of the A $\beta$  sequence, altered the binding properties of various antibodies to A $\beta$ , as analyzed by sandwich ELISA and immunohistochemistry (**Supplementary Fig. 11**). Antibodies to the N and C termini appeared to bind to both A $\beta$  species in a similar manner. Using an appropriate combination of the antibodies, we observed aggressive A $\beta$  amyloidosis in *App*<sup>NL-G-F/NL-G-F</sup> mice in an age-dependent manner (**Fig. 2a,b**). Notably, the cortical deposition began by 2 months and was almost saturated by 7 months. The heterozygous mice began A $\beta$  deposition at 4 months (**Supplementary Fig. 12**).

Unlike *App*<sup>NL-F/NL-F</sup> mice, *App*<sup>NL-G-F/NL-G-F</sup> mice also showed subcortical amyloidosis after 4 months (**Fig. 3b**), consistent with the pathology of human Arctic mutation carriers<sup>16</sup>. This subcortical amyloidosis was not detected in mice overexpressing human APP with the Arctic mutation, presumably because an artificial promoter was used to drive the transgene expression<sup>17</sup>. We observed greater microgliosis and astrocytosis in 9-month-old *App*<sup>NL-G-F/NL-G-F</sup> mice than in 18-month-old *App*<sup>NL-F/NL-F</sup> mice (**Fig. 2c**), implying that the Arctic A $\beta$  may be more proinflammatory than wild-type A $\beta$ . The reduction in synaptophysin and PSD95 immunoreactivities near A $\beta$  plaques was similar in these mutant mice (**Figs. 1e** and **2d**). Consistent with the pronounced A $\beta$  pathology, *App*<sup>NL-G-F/NL-G-F</sup> mice showed memory impairment by 6 months (**Fig. 2e**), approximately three times faster than *App*<sup>NL-F/NL-F</sup> mice.

The memory impairment that we observed in our mutant mice is likely to reflect preclinical cognitive decline in humans<sup>18</sup>. We therefore consider these mice to be useful tools for identifying and validating pathways by which A $\beta$  amyloidosis induces subsequent pathological changes. A number of approaches can now be adopted, including pathway analyses based on various 'omics' data. We can also analyze the tau interactome to identify protein(s) that may link A $\beta$  amyloidosis and tauopathy. In any case, the advantages lie in the existence of relevant negative controls and the lack of concern about overexpression artifact(s).

*App*<sup>NL-F/NL-F</sup> mice will also provide a better tool for identifying upstream factors that affect A $\beta$  amyloidosis than *App*<sup>NL-G-F/NL-G-F</sup> mice, given that the sequence of A $\beta$  is identical to that of wild-type A $\beta$ , which accumulates in most familial and sporadic AD patients.

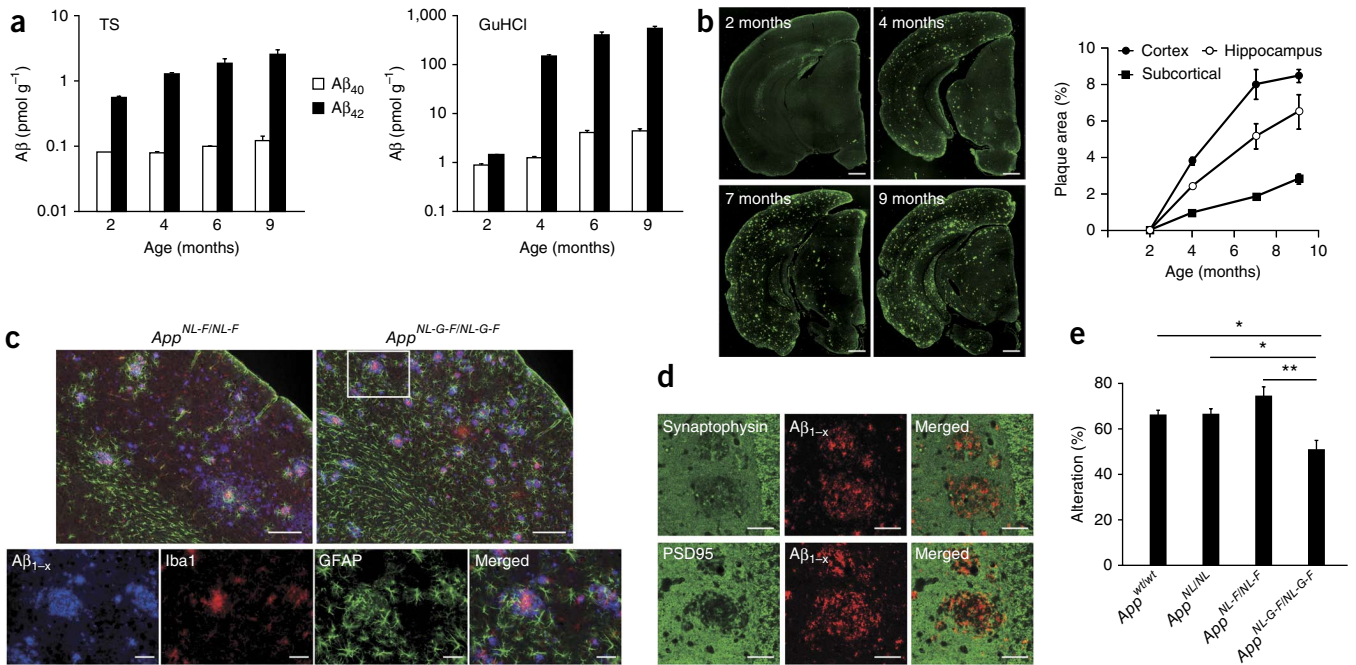


**Figure 2** Neuropathology and memory impairment of *App*<sup>NL-G-F/NL-G-F</sup> mice. (a) Biochemical quantities of A $\beta$  in *App*<sup>NL-G-F/NL-G-F</sup> brains. We quantified A $\beta$ <sub>40</sub> and A $\beta$ <sub>42</sub> in the TS and GuHCl fractions of cortex from 2–9-month-old mice by sandwich ELISA. We generated standard curves for calibration using synthetic A $\beta$ <sub>1–40</sub> and A $\beta$ <sub>1–42</sub> with E22G amino acid replacement (**Supplementary Fig. 11**). Data represent mean  $\pm$  s.e.m. ( $n = 4, 4, 6$  and  $6$  mice per indicated time point, respectively). (b) A $\beta$  deposition in *App*<sup>NL-G-F/NL-G-F</sup> brains. Brain sections from 2–9-month-old *App*<sup>NL-G-F/NL-G-F</sup> mice were immunostained using antibody to A $\beta$ <sub>42</sub>. Cortical, hippocampal and subcortical immunoreactive plaque areas were quantified as shown in the graph on the right ( $n = 3, 3, 4$  and  $4$  mice per indicated time point, respectively). Scale bars represent  $500 \mu\text{m}$ . (c) Neuroinflammation in *App*<sup>NL-G-F/NL-G-F</sup> mouse brains. Inflammatory responses were detected by triple staining of frozen sections from 18-month-old *App*<sup>NL-F/NL-F</sup> mice and from 9-month-old *App*<sup>NL-G-F/NL-G-F</sup> mice. Bottom, superimposed images of the boxed area in the upper right panel (*App*<sup>NL-G-F/NL-G-F</sup> mice) at a higher magnification. Cortical immunoreactivities were quantified as shown in **Supplementary Figure 10a**. Scale bars represent  $100 \mu\text{m}$  (top) and  $25 \mu\text{m}$  (bottom). (d) Synaptic alterations in *App*<sup>NL-G-F/NL-G-F</sup> mouse brains. Double staining was performed using antibody to A $\beta$ <sub>1-x</sub> with antibodies to synaptophysin and PSD95. Scale bars represent  $10 \mu\text{m}$ . (e) Memory impairment in *App*<sup>NL-G-F/NL-G-F</sup> mice. The Y-maze test was performed using 6-month-old mice. Data represent mean  $\pm$  s.e.m. ( $n = 10$  *App*<sup>wt/wt</sup>,  $9$  *App*<sup>NL/NL</sup>,  $9$  *App*<sup>NL-F/NL-F</sup> and  $10$  *App*<sup>NL-G-F/NL-G-F</sup>, one-way ANOVA with Sheffe's *F* test, \* $P < 0.05$  and \*\* $P < 0.01$ ).

It will be interesting to examine the phenotypes of *App*<sup>NL-F/NL-F</sup> mice lacking autophagosomal function, as *Atg7* deficiency induces impairment of A $\beta$  secretion, accumulation of intracellular A $\beta$  and neurodegeneration with no sign of tauopathy<sup>19</sup>, implying the presence of pathway(s) that lead from intracellular A $\beta$  to neurodegeneration independent of tauopathy. On the basis of these facts and assumptions, we propose that *App*<sup>NL-F/NL-F</sup> and *App*<sup>NL-G-F/NL-G-F</sup> mice be used as standard mouse models for identifying mechanisms and pathways upstream and downstream of A $\beta$  amyloidosis.

## METHODS

Methods and any associated references are available in the [online version of the paper](#).

Note: Any Supplementary Information and Source Data files are available in the [online version of the paper](#).

## ACKNOWLEDGMENTS

We thank C.A. Lemere (Brigham and Woman's Hospital) and M. Higuchi (National Institute of Radiological Science) for valuable discussions. We also thank E. Takano, R. Fujioka and Y. Tomita for technical assistance. This work was supported by research grants from RIKEN Brain Science Institute, the Ministry of Education, Culture, Sports, Science and Technology, the Ministry of Health and Welfare, grants-in-aid for the Molecular Imaging Program, Japan Science and Technology Agency Precursory Research for Embryonic Science and Technology, the Cell Science Research Foundation and the Takeda Science Foundation.

## AUTHOR CONTRIBUTIONS

This study was designed by T.S. and T.C.S. Generation of the knock-in mice was supported by S.I. Experiments were performed by T.S., Y.M., N.M. and J.T. T.S., J.T., P.N., N.I. and T.C.S. jointly analyzed and interpreted data.

## COMPETING FINANCIAL INTERESTS

The authors declare competing financial interests: details are available in the [online version of the paper](#).

Reprints and permissions information is available online at <http://www.nature.com/reprints/index.html>.

- Jonsson, T. *et al. Nature* **488**, 96–99 (2012).
- Hardy, J. & Allsop, D. *Trends Pharmacol. Sci.* **12**, 383–388 (1991).
- Hsiao, K. *et al. Science* **274**, 99–102 (1996).
- Sturchler-Pierrat, C. *et al. Proc. Natl. Acad. Sci. USA* **94**, 13287–13292 (1997).
- Citron, M. *et al. Nature* **360**, 672–674 (1992).
- Lichtenthaler, S.F. *et al. Proc. Natl. Acad. Sci. USA* **96**, 3053–3058 (1999).
- Guardia-Laguarta, C. *et al. J. Neuropathol. Exp. Neurol.* **69**, 53–59 (2010).
- Forman, M.S. *et al. J. Biol. Chem.* **272**, 32247–32253 (1997).
- Saido, T.C. *et al. Neuron* **14**, 457–466 (1995).
- Mitani, Y. *et al. J. Neurosci.* **32**, 2037–2050 (2012).
- Higuchi, M. *et al. FASEB J.* **26**, 1204–1217 (2012).
- Roberson, E.D. *et al. Science* **316**, 750–754 (2007).
- Liu, C.C., Kanekiyo, T., Xu, H. & Bu, G. *Nat. Rev. Neurol.* **9**, 106–118 (2013).
- Hashimoto, T. *et al. J. Biol. Chem.* **286**, 27081–27091 (2011).
- Tsubuki, S., Takaki, Y. & Saido, T.C. *Lancet* **361**, 1957–1958 (2003).
- Kalimo, H. *et al. Acta Neuropathol. Commun.* **1**, 60 (2013).
- Cheng, I.H. *et al. Nat. Med.* **10**, 1190–1192 (2004).
- Cash, D.M. *et al. Neurology* **81**, 1425–1433 (2013).
- Nilsson, P. *et al. Cell Reports* **5**, 61–69 (2013).

## ONLINE METHODS

**Generation of *App*<sup>NL/NL</sup>, *App*<sup>NL-F/NL-F</sup> and *App*<sup>NL-G-F/NL-G-F</sup> mice.** As described in **Supplementary Figure 1**, we isolated mouse *App* genomic DNA from the bacterial artificial chromosome (BAC) library carrying the C57BL/6 mouse genome, which included introns 15–17. We humanized the A $\beta$  sequence and introduced Swedish mutations into exon 16, and Beyreuther/Iberian and Arctic mutations into exon 17. Finally, we inserted a *pgk-neo* gene cassette with a lox/FRT sequence in intron 16 for positive selection. We used the fragment spanning intron 15 to exon 16 (genomic mouse *App* from 206,484 to 207,984; approximately 1.5 kbp) and the fragment spanning exon 17 to intron 17 (genomic mouse *App* from 210,922 to 216,617; approximately 5.7 kbp) as the short-arm and long-arm targeting vectors, respectively.

Embryonic stem (ES) cell culture and gene targeting were carried out as previously described<sup>20</sup>. Targeted ES cells were microinjected into C57BL/6 blastocysts. We extracted DNA from the biopsied tails of mouse pups and identified the F1 generation by Southern blotting using the following 5' and 3' external probes. The former was generated by PCR using a primer pair of 5'-ACCTGTTCCAATAACTCTACAGCC-3' and 5'-ATGTGGCAGTGACATGAATGCTC-3', and the latter by 5'-CACTCA CAGTCATTCACAGTGC-3' and 5'-GGCATCTACTTGTGTTCACAGCAC-3'.

We then crossbred heterozygous mutant mice with EIIa-Cre Tg mice to remove the *pgk-neo* gene. Finally, we removed the EIIa-Cre transgene by crossing the mice with wild-type C57BL/6 mice. We genotyped the mice by PCR using the following cocktail of primers: 5'-ATCTCGGAAGTGAAGATG-3', 5'-ATCTCGGAAGTGAATCTA-3', 5'-TGATAGAGAACCTTAAC-3' and 5'-CGTATAATGTATGCTATACGAAG-3'.

**Other mutant mice.** APP23 mice, which overexpress Swedish mutation-containing human APP751 under the control of the neuron-specific Thy-1 promoter, were maintained as previously described<sup>4</sup>. Calpastatin knockout (*Cast*<sup>-/-</sup>) mice have also been described previously<sup>20</sup>. All the mice used in the experiments were on the C57BL/6J background. All animal experiments were carried out according to the RIKEN Brain Science Institute's guidelines for animal experimentation.

**Northern blot analysis.** Total RNA from brain tissues were subjected to northern blotting to quantify APP expression levels using a North2South labeling and detection kit (Thermo Scientific), according to the manufacturer's instructions. Specific probes to identify the RNA of mouse *App* and *Actb* were produced by PCR using the following primer pairs: 5'-ATGTGCAGAATGGAAAGT-3' and 5'-CAGCATACAACTCTACC-3' for the former, and 5'-TCATGAAGTGTG ACGTTGACATCCGT-3' and 5'-CTTAGAAGCATTTGCGGTGCACGATG-3' for the latter. Full-length blots for this experiment are shown in **Supplementary Figure 13**.

**Western blot analysis of APP and APP-derived fragments.** Brain homogenates prepared as previously described<sup>21</sup> were subjected to western blotting using antibody to human A $\beta$ <sub>1–12</sub> (6E10, Covance), antibody to APP N terminus (22C11, Millipore) and antibody to APP-CTF (A8717, Sigma). Each set of experiments was repeated at least three times to confirm the results. The band intensity was determined with a densitometer, LAS4000 (Fujifilm). Full-length blots for these experiments are shown in **Supplementary Figure 14**.

**Enzyme-linked immunosorbent assay (ELISA).** Soluble materials from mouse cortical hemispheres were dissolved in TS fraction and insoluble materials in guanidine-HCl solution (GuHCl fraction) as previously described<sup>22</sup>. We quantified A $\beta$ <sub>X–40</sub> and A $\beta$ <sub>X–42</sub> in these fractions using an A $\beta$  ELISA kit (Wako) according to the manufacturer's instructions. We quantified A $\beta$ <sub>X–40</sub> and A $\beta$ <sub>X–42</sub> carrying the Arctic mutation based on standard curves using synthetic human Arctic A $\beta$  peptides (Peptide Institute).

**Immunohistochemical and histochemical studies.** We immunostained paraffin-embedded and frozen mouse brain sections using antibodies specific to the N termini of A $\beta$  (A $\beta$ <sub>1–X</sub> and A $\beta$ <sub>3(pE)–X</sub><sup>9</sup>), the N-terminal region of A $\beta$  (82E1, IBL), A $\beta$ <sub>17–24</sub> (4G8, Covance), A $\beta$ <sub>X–40</sub> (IBL), A $\beta$ <sub>X–42</sub> (IBL), phosphorylated tau (AT8, Invitrogen), synaptophysin (conjugated with FITC; clone SY38, PROGEN), the PSD95 PDZ domain (Synaptic Systems), Iba1 (Wako) and GFAP (MAB3402, Millipore). We used tyramide signal amplification (PerkinElmer Life Sciences), when necessary, as previously described<sup>23</sup>. 1-fluoro-2,5-bis(3-carboxy-4-hydroxystyryl)benzene (FSB) was used for detection of amyloidosis<sup>11</sup>. We performed antigen retrieval by autoclave (121 °C for 5 min) for 82E1 and 6E10 staining or by formic acid treatment (90% formic acid for 5 min at 20–25 °C) for immunohistochemistry of 4G8, A $\beta$ <sub>X–40</sub> and A $\beta$ <sub>X–42</sub> antibodies. We quantified the immunoreactive areas using MetaMorph imaging software (Universal Imaging) as previously described<sup>23</sup>. To reduce the variance among tissue sections, we used the average of data from at least four sections per mouse as an individual value.

**Y-maze and Morris water maze tests.** The Y-maze test was performed with a slight modification as previously described<sup>24</sup>. Mice were caged in a group of three to five individuals before transferring to a behavioral laboratory. The light condition was 12-h:12-h (lights on 8:00). All of the experiments were conducted in the light phase (9:00–18:00), and the starting time of the experiments was kept constant.

The Y-maze apparatus (O'Hara & Co), made of gray plastic, consisted of three compartments (3 cm (W) bottom and 10 cm (W) top, 40 cm (L) and 12 cm (H)) radiating out from the center platform (3 × 3 × 3 cm triangle), and positioned 60 cm above the floor. In this test, each mouse was placed in the center of the maze facing toward one of the arms and then allowed to explore freely for 5 min. The light intensity of the platform was kept at 80 lx. We recorded and analyzed the activity and spontaneous behavioral alternations of the mice using Time YM2 for Y-maze (Two Maze System, O'Hara & Co). A reduction in the behavioral alternations corresponds to memory impairment<sup>25</sup>.

The Morris water maze test was performed as previously described<sup>19</sup>, with minor modifications using Time MWM for the Morris water maze (O'Hara & Co). Although a tendency toward memory impairment was detected in 18-month-old *App*<sup>NL-F/NL-F</sup> mice, it did not reach statistical significance ( $P = 0.893$ ; data not shown).

**AD brain sections.** Postmortem AD brain tissues were kindly provided by J.Q. Trojanowski and V.M.-Y. Lee (University of Pennsylvania). The tissues had been fixed with ethanol or formalin and embedded in paraffin. Paraffin-embedded brain (neocortical and hippocampal region) sections from normal humans and AD patients were also purchased from Wako (Japan). The research plans to use human materials were approved by the Institutional Review Board of the RIKEN Brain Science Institute.

**Statistical analysis.** All data are shown as mean  $\pm$  s.e.m. For comparison between two groups, statistical analysis was performed by Student *t* test. For comparisons among three or more groups, we used one-way analysis of variance (ANOVA) or repeated-measures ANOVA followed by *post hoc* test (Scheffe *F* test). Normality was tested using Statcel 3 (add-in software for Excel, Microsoft). The data were collected and processed in a randomized and blinded manner. No statistical methods were used to predetermine sample size, but our sample sizes were similar to those generally employed in the field.

20. Takano, J. *et al. J. Biol. Chem.* **280**, 16175–16184 (2005).

21. Saito, T. *et al. Nat. Med.* **11**, 434–439 (2005).

22. Iwata, N. *et al. J. Neurosci.* **24**, 991–998 (2004).

23. Enya, M. *et al. Am. J. Pathol.* **154**, 271–279 (1999).

24. Saito, T. *et al. Nat. Neurosci.* **14**, 1023–1032 (2011).

25. Sarayai, Z. *et al. Proc. Natl. Acad. Sci. USA* **97**, 14731–14736 (2000).